Inversion of Borehole Guided Wave Amplitudes for Formation Shear Wave Attenuation Values

by

D.R. Burns and C.H. Cheng

Earth Resources Laboratory
Department of Earth, Atmospheric, and Planetary Sciences
Massachusetts Institute of Technology
Cambridge, MA 02139

ABSTRACT

A linear least squares inversion, based on analytic partition coefficient expressions, is developed to estimate the fluid and formation shear wave Q values from spectral ratio measurements of the guided wave arrivals of full waveform acoustic logs recorded in open boreholes. The method provides excellent results when applied to synthetic data. Real data applications provide useful results, but noise reduces the resolution and increases the variance of the estimates. Permeability related losses and transmission losses (if interfaces are present) can have large effects on the estimated values. A similar procedure is developed for cased hole geometries. In this situation, the guided wave measurements are used to provide estimates of the fluid, formation shear wave, and cement shear wave Q values. Application of the method to synthetic data indicates that the formation shear Q estimate is extremely sensitive to the pseudo-Rayleigh wave data quality very close to the cutoff frequency.

INTRODUCTION

Although surface geophysical measurements can provide much information on the nature of the earth's interior, data collected from boreholes drilled into the shallow crust provide direct knowledge about the geology of the subsurface. Rock cores extracted along the course of a borehole allow the actual geologic record to be examined in detail. Borehole geophysical measurements provide complementary information on the in-situ physical properties of the rocks in the subsurface, and also provide much needed calibration for any surface geophysical measurements. Borehole acoustic measurements are particularly

useful in providing information about the in-situ physical properties of the subsurface formations. Acoustic measurements are obtained by generating a pressure pulse along the axis of a fluid filled borehole and measuring the resulting pressure at several receivers situated on the axis some distance away. The most common method measures the travel time of the first arrival which travels at the P wave velocity of the formation along the borehole wall. By recording the entire wavefield, however, much additional information is gained. The first arrival of the full waveform acoustic log is the compressional head wave which propagates along the borehole wall. In most situations two other prominent arrivals are present: the pseudo-Rayleigh and Stoneley waves. These are borehole guided waves. The pseudo-Rayleigh wave is a dispersive wavetrain which is related to the fundamental and harmonic resonances of the borehole. The onset of this wave arrives at the shear wave velocity of the formation. The Stoneley wave is an interface wave which propagates along the borehole wall and is sensitive to the borehole fluid properties and the rigidity of the subsurface formations.

In most fast formation situations (that is, formation shear wave velocity greater than the borehole fluid velocity), the shear head wave is lost in the high amplitude pseudo-Rayleigh arrival, while in slow formations, no shear head wave (or pseudo-Rayleigh wave) is generated. As a result, the guided waves must be used to obtain formation shear wave Q (Q_β) estimates. The use of the guided waves is actually preferred since no corrections for geometrical spreading losses are required.

A knowledge of the in-situ P and S wave attenuation factors can provide qualitative information on the formation lithology, degree of consolidation, rock quality or fracture index, and possibly, the pore fluid saturation conditions (Johnston, 1978; Winkler and Nur, 1979; Toksöz et al., 1979; Johnston et al., 1979). The guided wave attenuation (both Stoneley and pseudo-Rayleigh) is controlled by the fluid Q value and the shear wave Q values of all solid layers in the borehole geometry. Estimates of the formation P wave Q value (Q_α), therefore, must be obtained by other means. The formation Q_α is generally estimated by spectral ratio methods applied to the earliest part of the P wave arrival (with appropriate spreading corrections applied) (Cheng et al., 1982). Cheng et al. (1986) have used the entire P - PL packet to obtain Q_α estimates from full waveform acoustic logs. In addition to the body wave Q effects, the Stoneley and pseudo-Rayleigh wave attenuation may also be affected by fluid flow in permeable formations (Rosenbaum, 1974; Williams et al., 1984; Schmitt, 1985; Cheng et al., 1987). Such losses are ignored in this paper. As will be demonstrated later, ignoring permeability related losses can result in errors being introduced in the calculated formation and fluid Q estimates. By assuming that the body wave Q values are frequency independent, partition coefficient expressions derived in Cheng et al.(1982) can be used to estimate the Q values of interest. In this paper an inverse problem, utilizing partition coefficients as the model, is formulated to obtain formation Q_β^{-1} and the fluid Q^{-1} from the measured attenuation (spectral ratios) of the Stoneley and pseudo-Rayleigh waves in open or cased boreholes.

PROBLEM FORMULATION

The attenuation of a guided wave is composed of a linear combination of the body wave attenuation values of the layers present in the borehole geometry, assuming all losses are due to layer anelasticity (Cheng et al., 1982). It is further assumed that all body wave Q values are frequency independent. By obtaining measurements of Stoneley and pseudo-Rayleigh wave attenuation over as broad a frequency range as possible, estimates of the body wave attenuation values can be obtained. As was shown in Burns et al. (1985), the guided waves are not sensitive to all Q values in a given layered model. In an open hole configuration, the guided wave attenuations are insensitive to the Q_α of the formation, while in cased hole geometries, they are insensitive to the Q_α of the cement, casing, and formation. Such insensitivity helps to simplify the inverse problem by reducing the number of parameters being solved for.

Previous Work

Cheng et al. (1982) and Willis (1983) outlined a method of estimating the formation shear wave attenuation (Q_β^{-1}) in open boreholes by using calculated partition coefficient expressions and measured spectral ratios of a given guided wave. Previous applications of the method, however, had two major problems. First, in order to separate the guided wave arrivals from the total trace, tapered variable length windows were used on the time domain record. Because of the relatively short receiver separations used in most full waveform acoustic logging tools (1 to 3 m), the arrivals are often interfering and difficult to separate. If, for example, the pseudo-Rayleigh wave has a well developed Airy phase, it will, in most cases, arrive after the Stoneley arrival. The pseudo-Rayleigh wave, then, arrives both before and after the Stoneley wave, resulting in the need for two windows to separate the wave from the remainder of the trace. The dispersive nature of the guided waves also requires that the time domain window lengths change between the near and far receiver traces. These complications make the application of such windowing extremely difficult.

The second problem faced in previous applications was narrow band data. In the past few years, the frequency band used in full waveform logging has increased in width. In particular, lower frequencies are being included which results in much more efficient excitation of the Stoneley wave. In the following section a method is proposed which can be applied to both open and cased hole geometries. The guided waves are separated in the frequency domain, and both the Stoneley and pseudo-Rayleigh waves are used simultaneously.

Inverse Problem Setup

It has been demonstrated (Burns, 1986) that the viscosity of the borehole fluid has a negligible effect on the guided wave propagation for the frequencies of interest in acoustic logging and reasonable values of fluid viscosity. In particular, the attenuation due to viscous drag along the borehole wall was found to be a minor component of the total guided wave attenuation. These results indicate that the assumption of frequency independent Q values is justified even for the borehole fluid. Using this assumption, then, the temporal Q^{-1} of a guided wave in a borehole can be represented (for small attenuation) by a linear combination of dissipation factors (body wave Q^{-1} values) for each layer through which it propagates. The weighting factors corresponding to these Q^{-1} values are the partition coefficients or normalized phase velocity partial derivatives. In Burns et al. (1985) analytic expressions, derived by Cheng et al. (1982), were presented and calculations were made for the Stoneley and pseudo-Rayleigh modes in a number of multilayered borehole geometries.

The temporal Q^{-1}, at angular frequency ω, for either guided wave in an open borehole can be represented by:

$$Q^{-1}(\omega) = \left[\frac{\alpha_f}{c}\frac{\partial c}{\partial \alpha_f}\right]_\omega Q_f^{-1} + \left[\frac{\alpha}{c}\frac{\partial c}{\partial \alpha}\right]_\omega Q_\alpha^{-1} + \left[\frac{\beta}{c}\frac{\partial c}{\partial \beta}\right]_\omega Q_\beta^{-1} \qquad (1)$$

and for a well bonded cased borehole by:

$$Q^{-1}(\omega) = \left[\frac{\alpha_f}{c}\frac{\partial c}{\partial \alpha_f}\right]_\omega Q_f^{-1} + \left[\frac{\alpha_{csg}}{c}\frac{\partial c}{\partial \alpha_{csg}}\right]_\omega Q_{\alpha_{csg}}^{-1} + \left[\frac{\beta_{csg}}{c}\frac{\partial c}{\partial \beta_{csg}}\right]_\omega Q_{\beta_{csg}}^{-1} \qquad (2)$$

$$+ \left[\frac{\alpha_{cmt}}{c}\frac{\partial c}{\partial \alpha_{cmt}}\right]_\omega Q_{\alpha_{cmt}}^{-1} + \left[\frac{\beta_{cmt}}{c}\frac{\partial c}{\partial \beta_{cmt}}\right]_\omega Q_{\beta_{cmt}}^{-1} +$$

$$\left[\frac{\alpha}{c}\frac{\partial c}{\partial \alpha}\right]_\omega Q_\alpha^{-1} + \left[\frac{\beta}{c}\frac{\partial c}{\partial \beta}\right]_\omega Q_\beta^{-1}$$

where the subscripts refer to:

$$f \qquad = \text{borehole fluid}$$
$$csg \qquad = \text{casing}$$
$$cmt \qquad = \text{cement}$$

(parameters with no subscripts refer to the formation). The partial derivatives, or partition coefficients, are functions of frequency. The results of Cheng et al. (1982) and Burns et al. (1985) allow us to simplify these equations. In the open borehole situation, only about 5% (or less) of the guided wave energy is in the form of compressional strain energy in the formation. The Q_α^{-1} term in Equation (1) can therefore be eliminated with minimal resulting errors. Similarly, in cased boreholes, the formation P-wave partition coefficient is small ($< 5 - 10\%$) and can be ignored. In addition, because steel casing has very high Q values in comparison to the other layers ($Q_{\alpha_{csg}} = Q_{\beta_{csg}} = 1000$ is the usual assumption), the casing terms in Equation (2) will have little affect on predicted dissipation of the guided wave and can be eliminated. Finally, the term in Equation (2) corresponding to the P-wave energy in the cement layer will also be eliminated because of its negligible effect (about 1% in most models). The resulting linear approximation for the open borehole geometry, then, is:

$$Q^{-1}(\omega) = \left[\frac{\alpha_f}{c} \frac{\partial c}{\partial \alpha_f} \right]_\omega Q_f^{-1} + \left[\frac{\beta}{c} \frac{\partial c}{\partial \beta} \right]_\omega Q_\beta^{-1} \qquad (3)$$

and for the cased borehole:

$$Q^{-1}(\omega) = \left[\frac{\alpha_f}{c} \frac{\partial c}{\partial \alpha_f} \right]_\omega Q_f^{-1} + \left[\frac{\beta_{cmt}}{c} \frac{\partial c}{\partial \beta_{cmt}} \right]_\omega Q_{\beta_{cmt}}^{-1} + \left[\frac{\beta}{c} \frac{\partial c}{\partial \beta} \right]_\omega Q_\beta^{-1} \qquad (4)$$

The error in guided wave Q^{-1} due to these simplifications is about 2-3 percent for the open hole geometry, and about 5-7 percent for the cased hole geometry.

In a fast formation (open or cased), the Stoneley wave is most sensitive to the fluid Q value, while the pseudo-Rayleigh wave, near the cutoff frequency, is most sensitive to the formation shear wave Q value. In a slow formation, the Stoneley wave becomes quite sensitive to the formation shear wave Q. In general, we are most interested in the estimation of the formation shear wave Q value. In fast formation situations, then, both the Stoneley and pseudo-Rayleigh wave amplitude information will be used, while in a slow formation, only the Stoneley wave information is available. It should also be noted that the shear wave Q value of the cement layer in the cased borehole formulation may be of some interest as an indicator of the cement quality or the presence of channeling (i.e., zones of non-existent or poorly cured cement along which fluids may migrate).

The inverse problem can now be set up. By using Stoneley and pseudo-Rayleigh wave information (when available) simultaneously and measuring spectral ratios for each wave over as wide a frequency range as possible, an over determined system of linear equations results which takes the form:

$$Ax = b \qquad (5)$$

where:

A = N x M matrix composed of calculated partition coefficients
x = M x 1 parameter vector (layer dissipation factors)
b = N x 1 data vector (guided wave dissipation values)

The N equations represent N frequency values of the Stoneley wave for a slow formation. For a fast formation, however, the structure of the system is:

$$\begin{matrix} N_1 \\ N_2 \end{matrix} \begin{bmatrix} A_{St} \\ A_{pR} \end{bmatrix} x = \begin{bmatrix} b_{St} \\ b_{pR} \end{bmatrix} \begin{matrix} N_1 \\ N_2 \end{matrix} \qquad (6)$$

where:

N_1 = number of Stoneley wave frequency values
N_2 = number of pseudo-Rayleigh wave frequency values
b_{St} = Stoneley wave dissipation data
b_{pR} = pseudo-Rayleigh wave dissipation data
A_{St} = Stoneley wave partition coefficients
A_{pR} = pseudo-Rayleigh wave partition coefficients

A solution to Equation (5) is obtained by using a special case of the stochastic inverse (Aki and Richards, 1980). The stochastic inverse is a least squares solution which includes the statistical aspects of both the data and the model. If the model and data covariances can each be represented by a constant variance times the identity matrix, the damped least squares solution emerges (Aki and Richards, 1980):

$$\hat{x} = (A^T A + \epsilon^2 I)^{-1} A^T b \qquad (7)$$

where:

$$\epsilon^2 = \frac{\sigma_b^2}{\sigma_x^2}$$

and:

$$\sigma_b^2 \qquad = \text{data variance}$$
$$\sigma_x^2 \qquad = \text{model (parameter) variance}$$

The damping factor(ϵ^2) ensures that the matrix ($A^T A$) is non-singular by suppressing the contributions of eigenvectors whose eigenvalues are less than ϵ^2 (Wiggins, 1972; Aki and Richards, 1980). The damped least squares solution can also be derived by solving the least squares problem subject to a bounding constraint on the sum of squared errors. This approach is referred to as the Levenburg-Marquardt method (Lines and Treitel, 1984). The addition of a damping term prevents the solution from being dominated by small eigenvalue directions which are very sensitive to the presence of noise.

Several additional calculations can be made to try to characterize the solution $\hat{x}$. First, the parameter resolution is calculated. Substituting Equation (5) into Equation (7) results in:

$$\hat{x} = Rx \qquad (8)$$

The parameter resolution matrix (R) provides a measure of how well the parameter estimation $\hat{x}$ matches the actual (unique) least squares solution. The second calculation to be performed is to see how well the model response matches the data. The predicted model behavior is given by:

$$A\hat{x} = \hat{b} \qquad (9)$$

which, together with Equation (7), yields:

$$\hat{b} = Sb \qquad (10)$$

S is a measure of the model resolution in data space (Wiggins, 1972). The closer the matrix is to the identity matrix, the better the agreement between the model and data. Finally, the parameter covariance matrix (σ_x^2) is calculated to give some measure of the error in parameters due to errors (noise) in the data (Aki and Richards, 1980).

The parameter and data resolution matrices and the covariance matrix for the damped least squares solution are given by:

$$R = (A^T A + \epsilon^2 I)^{-1} A^T A \qquad (11)$$

$$S = A(A^T A + \epsilon^2 I)^{-1} A^T \qquad (12)$$

$$\sigma_x^2 = \sigma_b^2 (A^T A + \epsilon^2 I)^{-1} A^T A (A^T A + \epsilon^2 I)^{-1} \qquad (13)$$

The data variance can be estimated by (Wiggins, 1972):

$$\sigma_b^2 = \frac{\left| b - \hat{b} \right|^2}{N - M} \qquad (14)$$

That is, the final squared error between the model and data is assumed to be due to noise or errors in the data.

As ϵ^2 increases, the parameter covariance decreases, but the resolution of the solution is also reduced. The selection of an appropriate damping factor is made by weighing the trade off between parameter resolution and variance. As will be seen in the next section, the inversion of noise free synthetic data can be carried out with $\epsilon^2 = 0$, but real data will usually require some damping due to the presence of noise.

INVERSION RESULTS

Synthetic Data

In order to fully explain the exact procedure used to obtain attenuation estimates, and to investigate the accuracy and sensitivity of the results in a controlled situation, the inversion procedure is first carried out on synthetic data for an open and cased borehole geometry. A flow chart of the computational procedure is given in Figure 1. The data vector is constructed from the spectral ratios of the Stoneley and pseudo-Rayleigh waves over a range of frequency values. The spectral ratios are converted to temporal Q^{-1} values by:

$$Q^{-1}(f) = U \frac{ln(A_{near}/A_{far})}{\pi f \Delta z} \tag{15}$$

where:

f	= frequency
A_{near}	= near receiver spectral amplitude at frequency f
A_{far}	= far receiver spectral amplitude at frequency f
Δz	= receiver separation
U	= group velocity at frequency f

The group velocity used in Equation (15) is calculated analytically from the input model parameters. The model matrix, which consists of calculated partition coefficients, is then generated. The resulting system of linear equations is solved for the parameters of interest (Q_f^{-1} and Q_β^{-1} in an open hole geometry; Q_f^{-1}, Q_β^{-1} and $Q_{\beta_{cmt}}^{-1}$ in a cased hole geometry) by using the damped least squares method.

Synthetic data from Tubman (1984) is used to test the routine. The data was generated by the discrete wavenumber method (White and Zechman, 1968; Cheng and Toksöz, 1981) for a fast formation in an open and cased hole situation. The open hole data for two offsets is shown in Figure 2, while the cased hole data is given in Figure 6. The parameters used to generate the data are given in Table 1. The source wavelet is a 13kHz center frequency damped sinusoidal signal used by Tsang and Rader (1979). In both examples, the 3.05m (10') and 4.57m (15') source-receiver offsets are used as the near and far receiver traces for input into the inversion procedure.
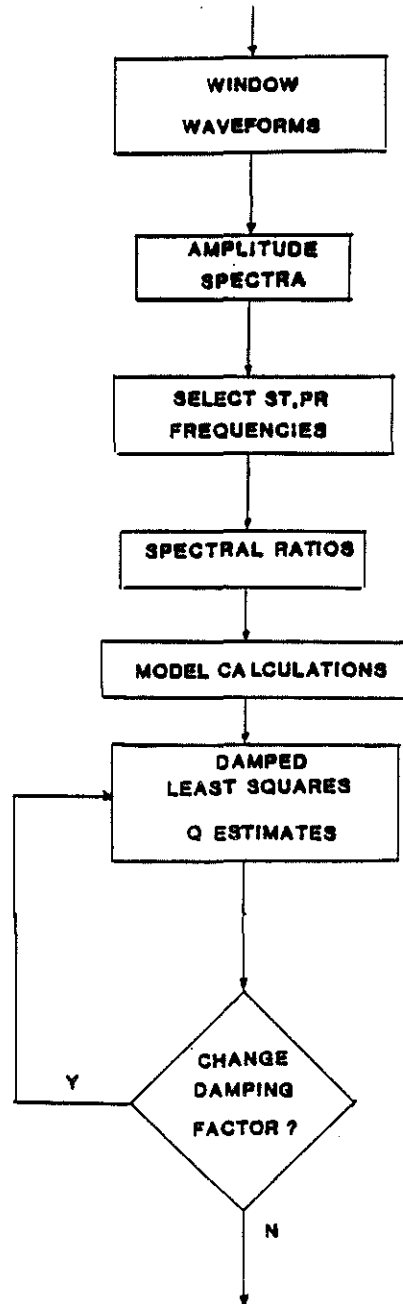
Figure 1: Flow chart of the computational procedure used to estimate attenuation factors

Table 1: Modelling parameters used to generate the synthetic data

LAYER	V_p (m/sec)	V_s (m/sec)	ρ (g/cm^3)	Q_α	Q_β
fluid	1676	0	1.2	20	0
formation	4878	2601	2.16	60	60
casing	6098	3354	7.5	1000	1000
cement	2823	1729	1.92	40	30

Open Hole

The two traces used in the open hole inversion are shown in Figure 2 with the start of the guided wave window noted on each trace. The amplitude spectra of the two traces are shown in Figure 3. Note that although the Stoneley and pseudo-Rayleigh waves are difficult to separate in the time domain, separation in the frequency domain is fairly straight forward. The spectral ratios are given in Figure 4 with the selected frequency ranges for each wave indicated. The inversion results obtained for this example are:

$$Q_f^* = 19.5 \tag{16}$$

$$Q_\beta^* = 59.1$$

As noted in Table 1, the actual Q values used to generate the synthetic traces are:

$$Q_f = 20 \tag{17}$$

$$Q_\beta = 60$$

The predicted results are in excellent agreement with the actual values. The small differences can be attributed to the fact that the formation compressional wave Q effects have been neglected in the model. The predicted values were calculated without damping, and as such, are perfectly resolved (Equation 11).

The frequency ranges chosen for the spectral ratios of the two wave types warrant some discussion. For the Stoneley wave, the frequency range chosen is not critical (for
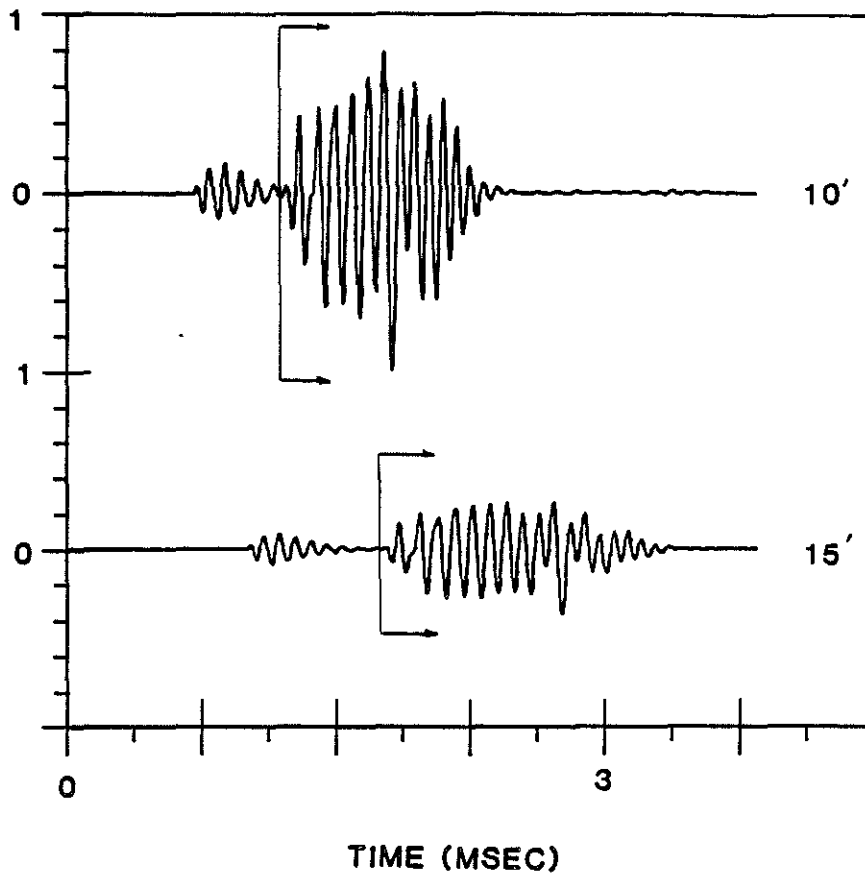
Figure 2: Synthetic microseismograms for an open borehole with a fast formation. The two offsets are 3.05m (10') and 4.57m (15'). The start of the guided wave window is noted on each trace
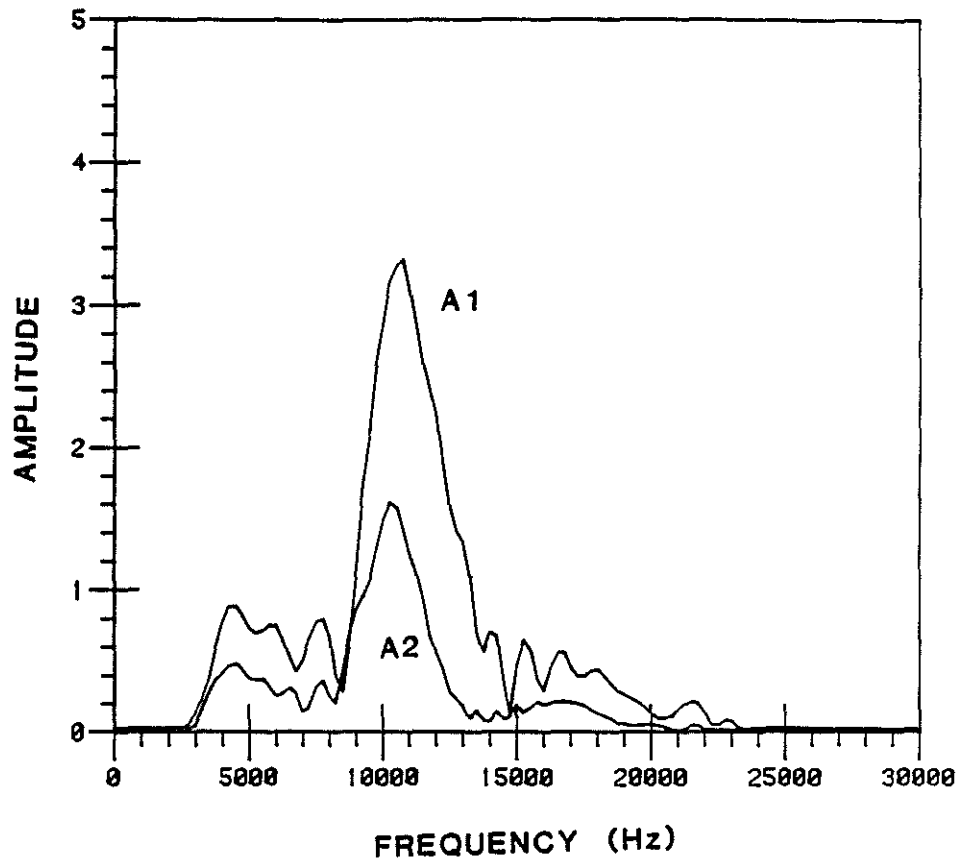
Figure 3: Amplitude spectra for the guided wave portions of the synthetic microseismograms given in Figure 2
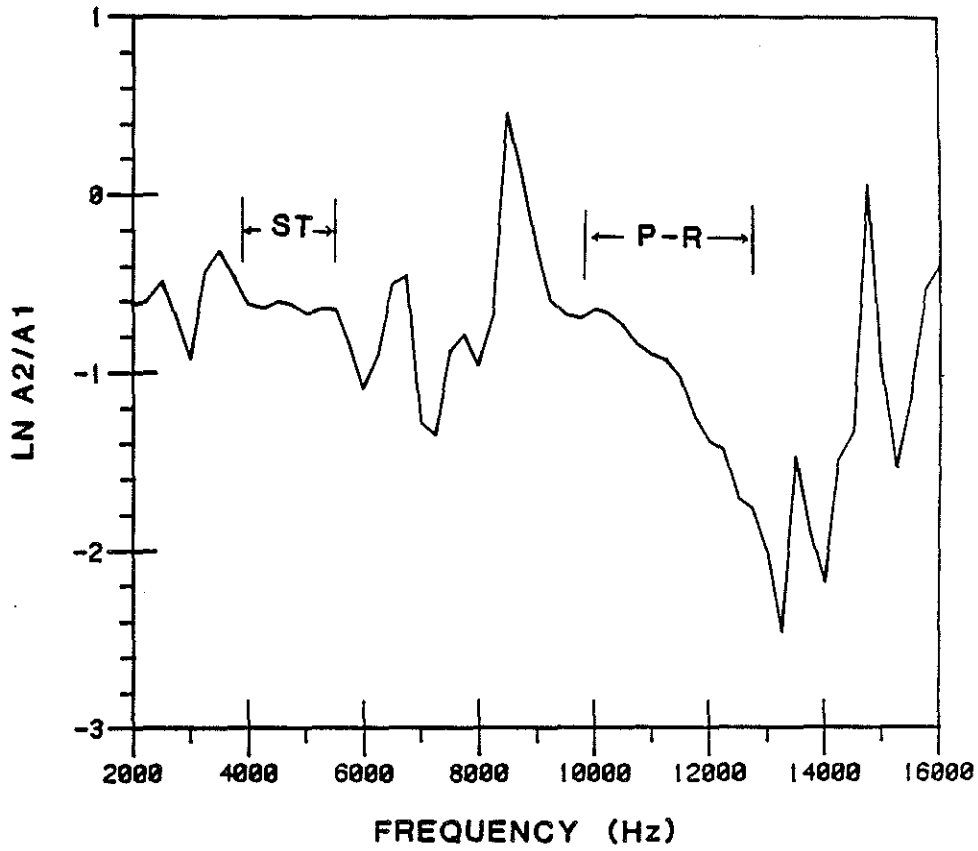
Burns and Cheng

Figure 4: Spectral ratios obtained from the spectra in Figure 3. The frequency ranges for the Stoneley and pseudo-Rayleigh waves are indicated

the fast formation situation) since the partition coefficients show very little variation with frequency (Figure 5). The partition coefficients for the pseudo-Rayleigh wave, however, change rapidly for frequencies between the cutoff frequency and the Airy phase frequency (Figure 5). The pseudo-Rayleigh wave is very sensitive to the formation shear wave Q value at frequencies close to the cutoff frequency. As a result, a better estimate of the formation Q_β can be obtained if spectral ratio values close to the cutoff frequency are used in the inversion. The cutoff frequency of the fundamental mode of the pseudo-Rayleigh wave is calculated within the inversion routine based on the model parameters supplied. (This calculation is performed by solving the period equation for the frequency at which the phase velocity equals the formation shear velocity.) The spectral ratios of the pseudo-Rayleigh wave can then be chosen as close to the cutoff frequency as possible. The calculation of the cutoff frequency also provides a check on the accuracy of the input model parameters, particularly the borehole radius, fluid velocity, and shear velocity, since the calculated cutoff frequency can be compared with the value which is evident from the amplitude spectrum of the data. In Figure 3, the amplitude spectra of the data traces indicate that the cutoff frequency is between 8 and 9 kHz, while the calculated value is 8.44kHz, indicating that the input parameters are in good agreement with the data.

The inversion results for this open hole synthetic example are excellent, but the data is noise free and all the model parameters are exactly known. Although the presence of noise in the data will certainly degrade the results, this degradation will be reflected in the calculated solution variances. A more critical question involves the degradation of the solution due to errors in the 'known' model parameters, that is, the parameters used to generate the partition coefficients. These parameters are (for the open borehole): the fluid velocity and density, the formation P and S wave velocities and density, and the borehole radius. The partition coefficient curves (Figure 5) indicate that the Stoneley wave attenuation is primarily controlled by the fluid attenuation at all frequencies (for a fast formation), while the pseudo-Rayleigh wave is controlled by the formation shear wave attenuation at low frequencies and the fluid attenuation at high frequencies. The estimated values of Q_β, then, will be controlled by the low frequency behavior of the pseudo-Rayleigh wave partition coefficients, and any errors in model parameters which affect the partition coefficient calculations in this region could greatly affect the formation shear wave Q estimates. The fluid Q, on the other hand, should be very robust to errors in model parameters since the estimated value is controlled by the Stoneley wave partition coefficient behavior which is quite insensitive to model variations.

To quantify the sensitivity of the Q estimates to model parameter errors, the inversion procedure has been repeated with the key model parameters perturbed by 5-10% about their actual values. The resulting solutions are given in Table 2. Again, no damping was utilized in the inversion. In general, the estimated fluid Q, as expected, is very insensitive to parameter errors, while the formation Q_β value is very sensitive to errors in parameters which change the predicted cutoff frequency or shape of the partition
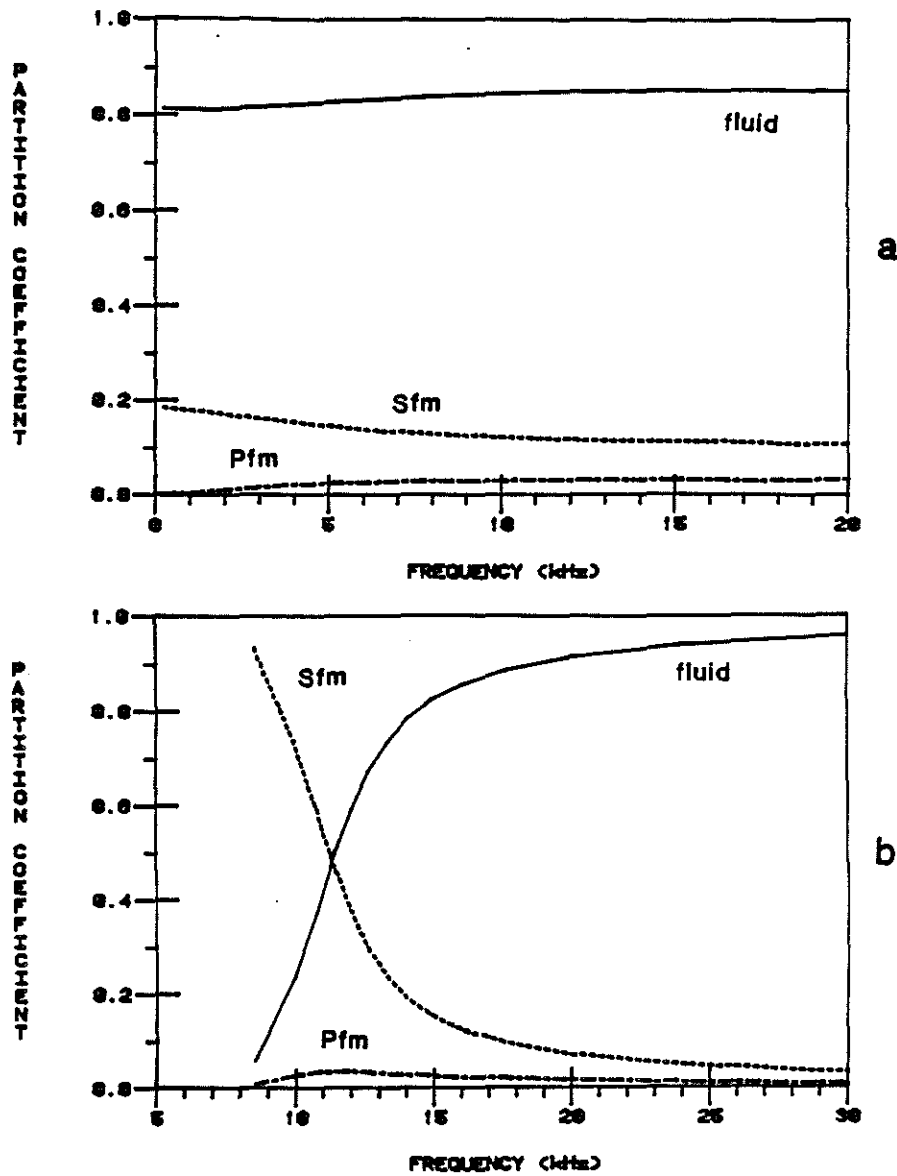
Burns and Cheng

Figure 5: Partition coefficient curves for the open borehole synthetic example. (a) Stoneley wave and (b) pseudo-Rayleigh wave. P_{fm} and S_{fm} refer to the compressional and shear wave partition coefficients in the formation, and *fluid* refers to the compressional wave partition coefficient in the fluid

Table 2: Sensitivity of synthetic data estimated Q values to model parameter perturbations

parameter varied	Q_f	Q_β
none	19.5	59.1
V_s (-5%)	19.05	51.9
V_s (+5%)	19.9	68.9
V_f (-5%)	20.6	985.
V_f (-10%)	21.2	-31.7
R (-5%)	19.7	38.9
R (+5%)	19.0	171.1
ρ (-5%)	19.3	65.5
ρ (+5%)	19.6	54.5

coefficient curves. The Q_β estimates are particularly sensitive to the fluid velocity and borehole radius.

All of these calculations were carried out for parameter variations of 5-10% about the actual values to compare the relative effects of errors in different parameters. The expected errors for these parameters, however, are generally less than 5%. Formation shear velocity can be measured with an accuracy of a few percent (Willis and Toksöz, 1983). Fluid velocity, although seldom measured, is fairly well constrained and can be estimated based on the fluid composition and density (which are measured). The fluid velocity generally varies between about 1480 m/sec for fresh water to about 1680 m/sec for very dense drilling fluid, a difference of 12%. Given knowledge of the fluid density and composition, however, the velocity can be estimated to within a few percent. The formation Q_β estimates are also very sensitive to errors in the borehole radius. Caliper logs, however, are routinely available to provide information on the hole size. Data from zones displaying large borehole size variations should be avoided.

Cased Hole

The second synthetic example is for a cased hole geometry. The parameters used to generate the synthetic data are given in Table 1. The two traces used in the inversion are shown in Figure 6. The start of the guided wave window is also noted on this figure. The amplitude spectra for these traces are given in Figure 7, while the spectral ratios and selected frequency ranges are shown in Figure 8. The inversion results (no damping) for this example are:
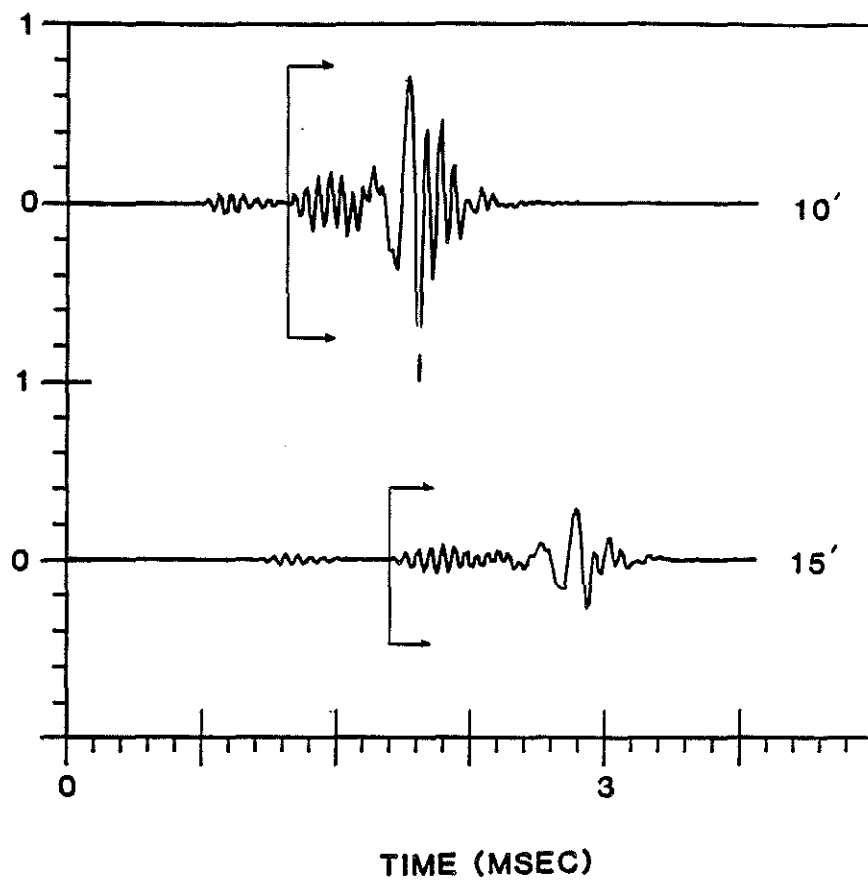
Figure 6: Synthetic microseismograms for a cased borehole with a fast formation. The two offsets are 3.05m (10') and 4.57m (15'). The start of the guided wave window is noted on each trace
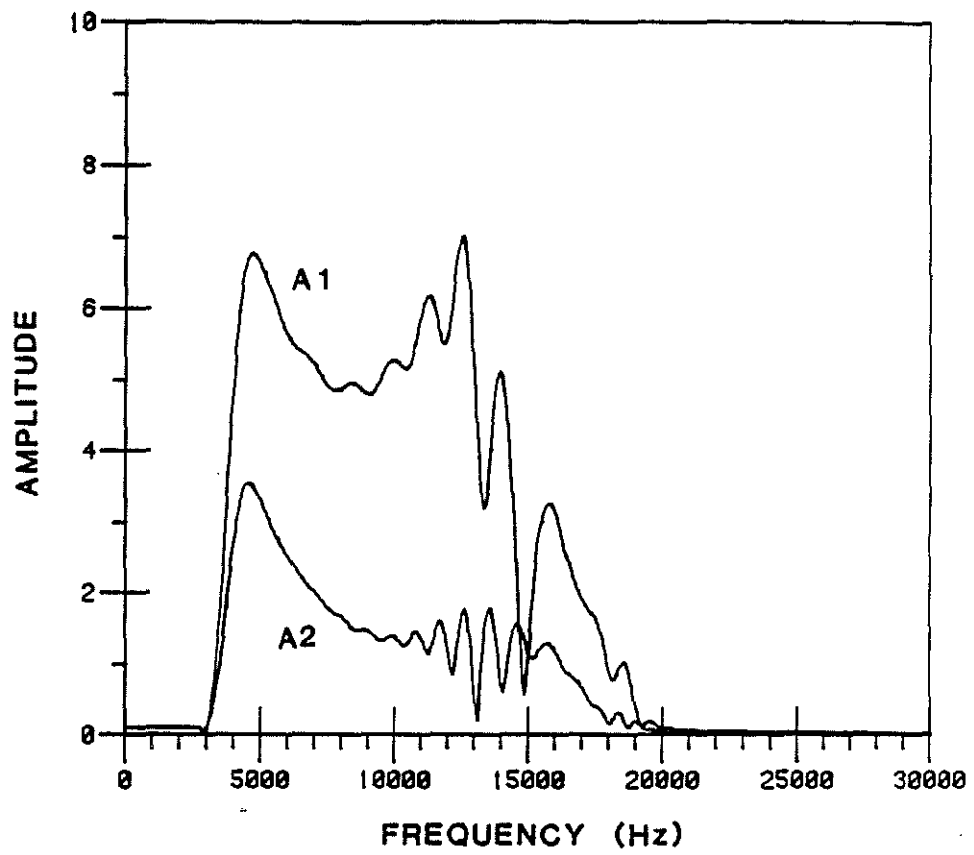
Figure 7: Amplitude spectra for the guided wave portions of the synthetic microseismograms given in Figure 6
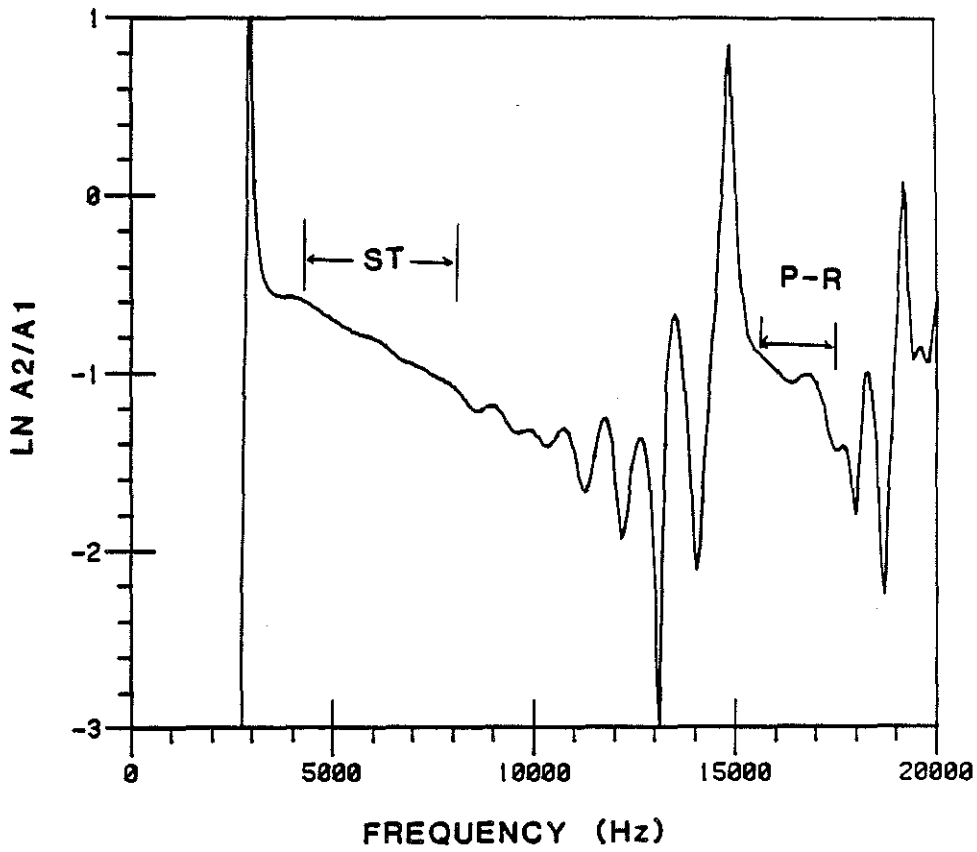
Burns and Cheng

Figure 8: Spectral ratios obtained from the spectra in Figure 7. The frequency ranges for the Stoneley and pseudo-Rayleigh waves are indicated

$$Q_f^* = 20.7 \tag{18}$$

$$Q_\beta^* = 43.8$$

$$Q_{\beta_{cmt}}^* = 29.$$

while the actual values are:

$$Q_f = 20 \tag{19}$$

$$Q_\beta = 60$$

$$Q_{\beta_{cmt}} = 30$$

The estimates in this case are excellent for the fluid and cement shear Q values, but in error by about 25% for the formation shear Q value. This error is the result of not selecting frequencies close enough to the cutoff frequency. The cutoff frequency for this example is about 13kHz, although the identifiable pseudo-Rayleigh mode in Figure 7 appears to have a cutoff frequency of about 15kHz (it is possible that the notch in the amplitude spectrum at about 13kHz may represent the pseudo-Rayleigh wave cutoff). Data resolution calculations (Equation 12) indicate that the model can only match the average of the Stoneley wave data attenuation. The Stoneley wave Q^{-1} is invariant with frequency in a cased hole situation and is controlled by the fluid Q^{-1} value. The pseudo-Rayleigh wave provides the information for estimating the formation and cement Q values due to its varying depth of investigation. At frequencies very close to the cutoff frequency, the pseudo-Rayleigh attenuation is most sensitive to the formation shear wave Q, at intermediate frequencies it is most sensitive to the cement shear wave Q, and at high frequencies it is most sensitive to the fluid Q value. The presence of the casing and cement layers results in a rapid decrease in the sensitivity to formation Q_β as the frequency increases. This behavior is seen in the partition coefficient curves shown in Figure 9. Such a rapid change in the partition coefficient values for the pseudo-Rayleigh wave indicates that the Q_β estimate in a cased hole situation will be very sensitive to the data quality near the cutoff frequency.
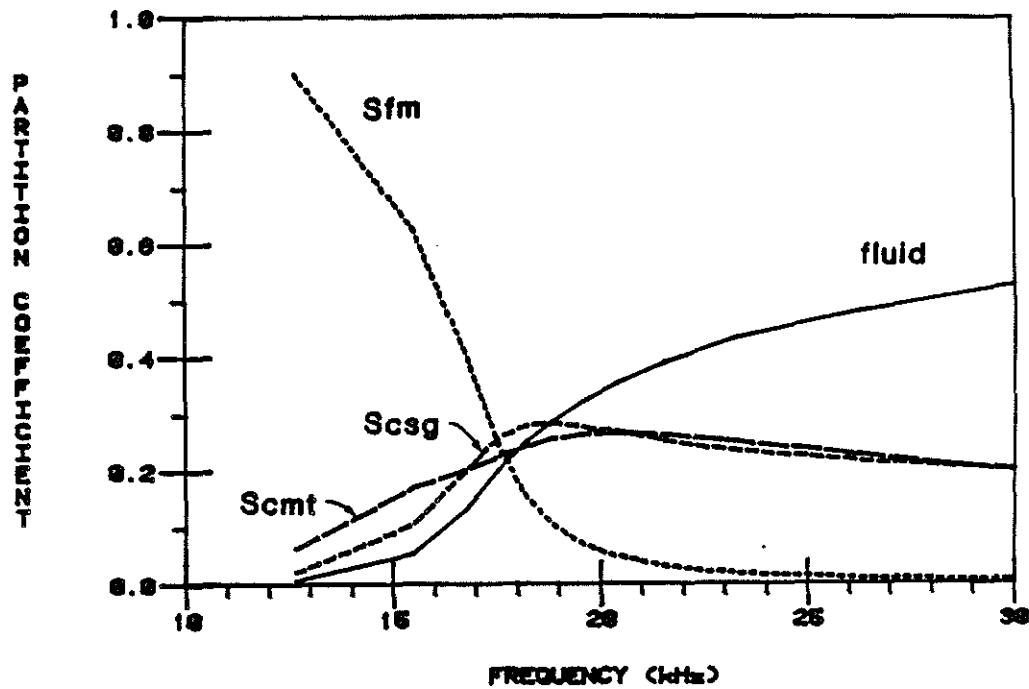
Figure 9: Pseudo-Rayleigh wave partition coefficient curves for the cased borehole synthetic example. P_{fm} and S_{fm} refer to the compressional and shear wave partition coefficients in the formation, S_{csg} and S_{cmt} refer to the shear wave partition coefficients in the casing and cement layers respectively, and $fluid$ refers to the compressional wave partition coefficient in the fluid

It is clear from the results of the synthetic cased hole example that the cutoff frequency may not be easily identified in multilayered borehole situations. By using data for frequencies higher than the cutoff frequency, the formation shear wave Q estimates become less reliable, although the fluid and cement Q estimates remain quite good.

Real Data Applications

In this section the inversion procedure is applied to actual field data. Two sets of full waveform acoustic log data collected in an open hole geometry are used, one collected in a sand-shale lithologic sequence, and a second collected in a limestone-dolomite sequence.

Sand/Shale Example

The first example consists of a data set which was collected in a small diameter borehole (0.13 m (5")) which penetrated a fairly low velocity sand-shale sequence. The borehole was drilled as part of a uranium leaching project. Full waveform data was selected throughout the interval between 588 m (1930') and 640 m (2100') representing both the sand and shale intervals. Figure 10 shows the full waveform traces corresponding to a single source receiver offset for this total interval. The data are relatively noise free so the data selection process was based on the reliability of supporting data (such as formation velocity values) rather than careful screening based on data quality. Table 3 provides a list of the depths chosen for analysis, together with the input model parameters for each depth. Formation shear wave velocity was obtained from a shear wave logging tool (Zemanek et al., 1984) run in the same borehole. The borehole was reported to contain only water which is estimated to have a velocity of 1475 m/sec and a density of 1.05 gm/cc. The formation density has been estimated to be 2.16 gm/cc for the sand units and 2.4 gm/cc for the shale units. The density of the sand zones is based on an assumed porosity of 30% and a quartz matrix material having a density of 2.65 gm/cc. The source-receiver offsets for the near and far receivers are 4.57m (15') and 6.1m (20') respectively. The near and far offset data traces for two of the depths analyzed are shown in Figure 11. In some of the traces in Figure 10 an arrival is present before the Stoneley wave which is similar in appearance to a pseudo-Rayleigh wave. The velocity of this arrival is consistent with the formation shear wave velocity as measured with the shear wave acoustic logging tool, and is most likely a shear head wave arrival. The shear head wave arrival is usually overwhelmed by the high amplitude pseudo-Rayleigh wave arrival but is visible in this data because of the small borehole radius. The small radius results in a high cutoff frequency for the pseudo-Rayleigh wave (12-14kHz) which is not excited by the low frequency source of the tool (centered at 3-6kHz). The shear head wave is visible in the zones having shear velocity greater than the borehole fluid
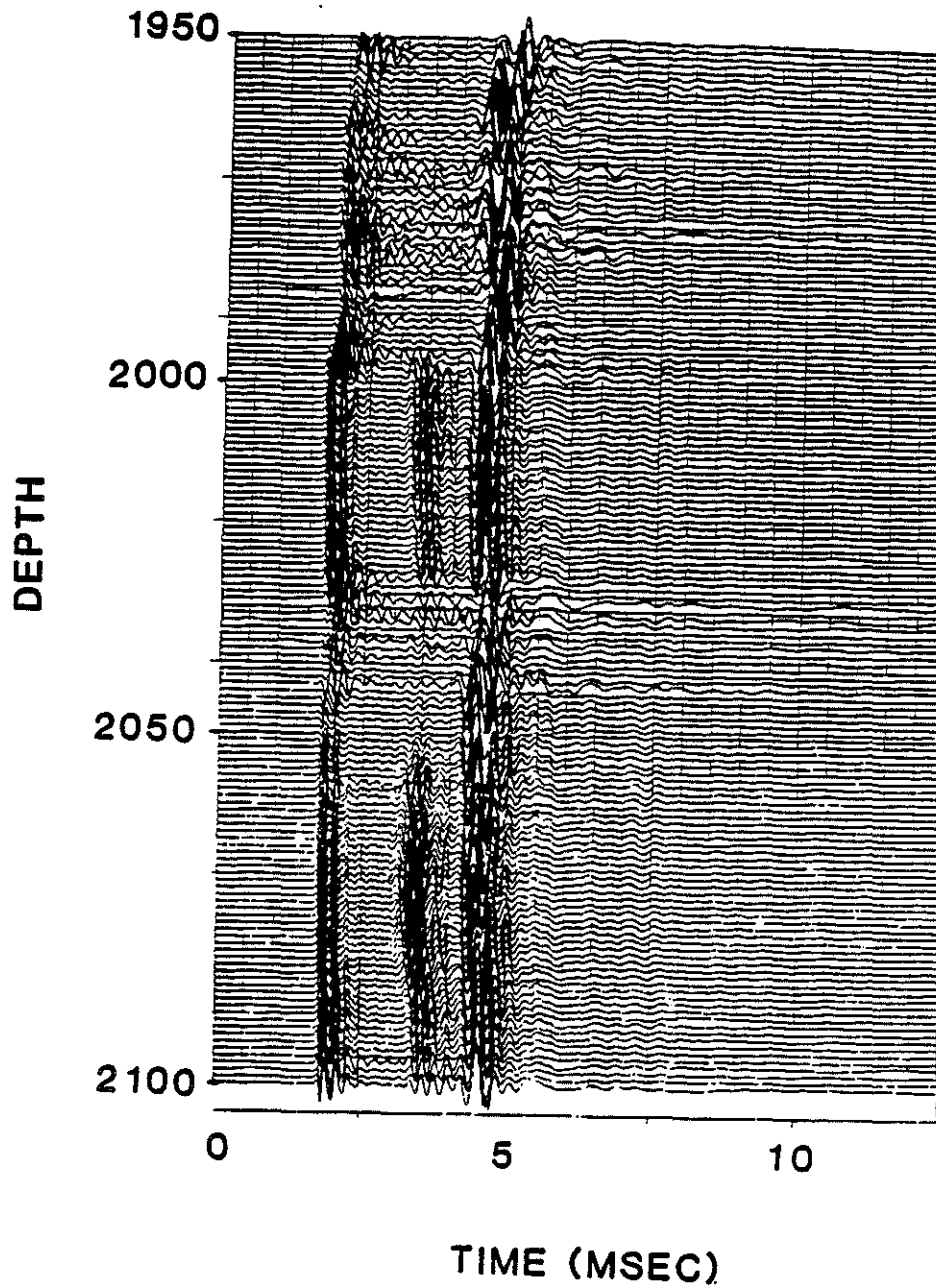
Figure 10: Iso-offset plot of the full waveform acoustic logging data for the sand/shale example. The offset is 4.57m (15')
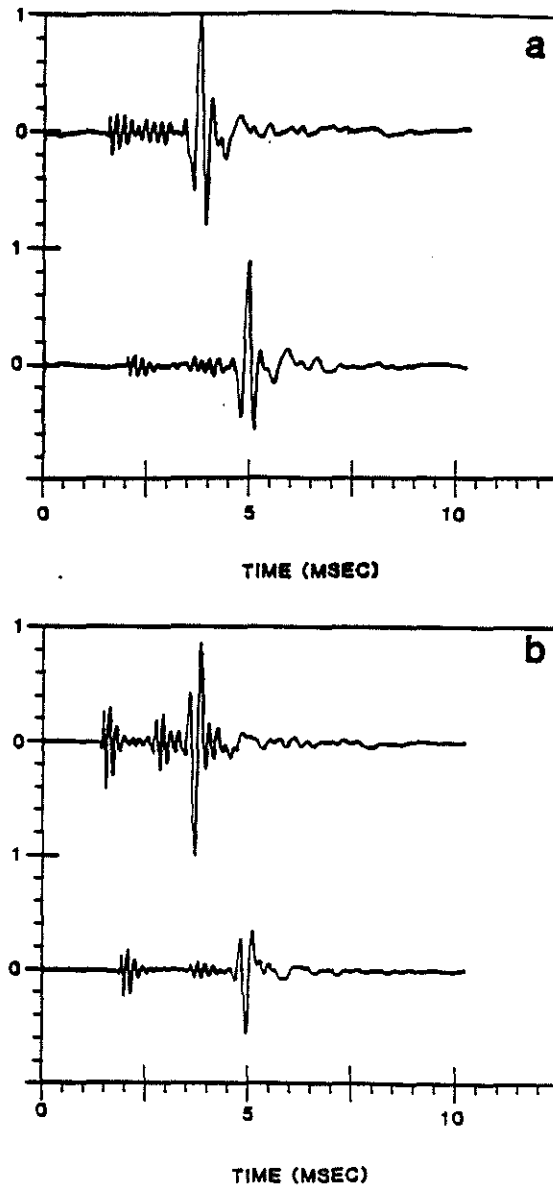
Figure 11: Near (4.57m, 15') and far (6.1m, 20') offset traces for two depths of the sand/shale example full waveform acoustic log data: (a) depth 1970 and (b) depth 2020. Both traces in each example are normalized to the maximum amplitude of the near offset trace

Table 3: Depth and model parameters used for the sand/shale data example

DEPTH	V_p (m/sec)	V_s (m/sec)	ρ (g/cm^3)
1920	2772	1463	2.4
1930	3278	1524	2.4
1946	2772	1463	2.4
1970	3209	1591	2.4
2000	3314	1925	2.16
2003	3388	1829	2.16
2010	3278	1829	2.16
2020	3314	1742	2.16
2035	3504	1663	2.4
2040	3587	1709	2.4
2050	3388	1663	2.16
2070	3504	1829	2.16
2090	3426	1742	2.16

velocity and not present in the 'slow' shale intervals (Figure 10). Figure 12 shows the amplitude spectra and spectral ratios at one depth to illustrate the frequency band and the quality of the data.

The inversion results for these data are given in Table 4. In each case, a small amount of damping was used to stabilize the inversion. The amount of damping, which was generally less than 1-2% of the largest diagonal element of $A^T A$, was chosen to maintain positive Q values and keep the resolution as high as possible. Figure 13 is a plot of the calculated Q^{-1} values with error bars representing +- one standard deviation about the estimated value. Borehole measurements of spontaneous potential and resistivity are also shown in this figure.

The inversion results for this data set are very dependent on the lithology. In the shale sections, the fluid Q estimates are high (150-250) and the formation shear wave Q estimates are fairly low (20-30). In the sand sections, however, both estimates are low (fluid Q = 20-40; formation shear Q = 20-40). It is reasonable to expect the fluid Q value to be high in this well because the borehole was filled with water. Even the fluid Q values obtained in the shale sections are lower than one would expect (Q of water is on the order of 10000). However, it is likely that the borehole fluid is more like a suspension containing clay and sand particles entrained in the fluid during the drilling and logging operations. It is disturbing, however, that the fluid Q estimates in the sand intervals are not consistent with the shale results. This inconsistency can be attributed
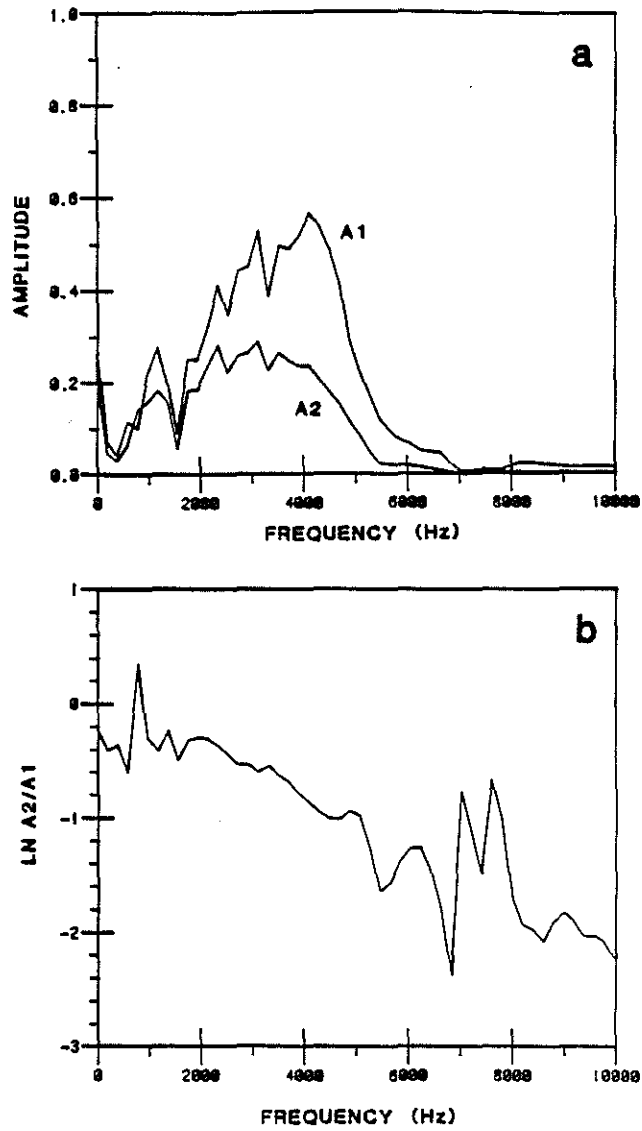
Figure 12: Amplitude spectra (a) and spectral ratios (b) for the data at depth 2020 in the sand/shale example. A1 refers to the near receiver amplitude and A2 refers to the far receiver amplitude
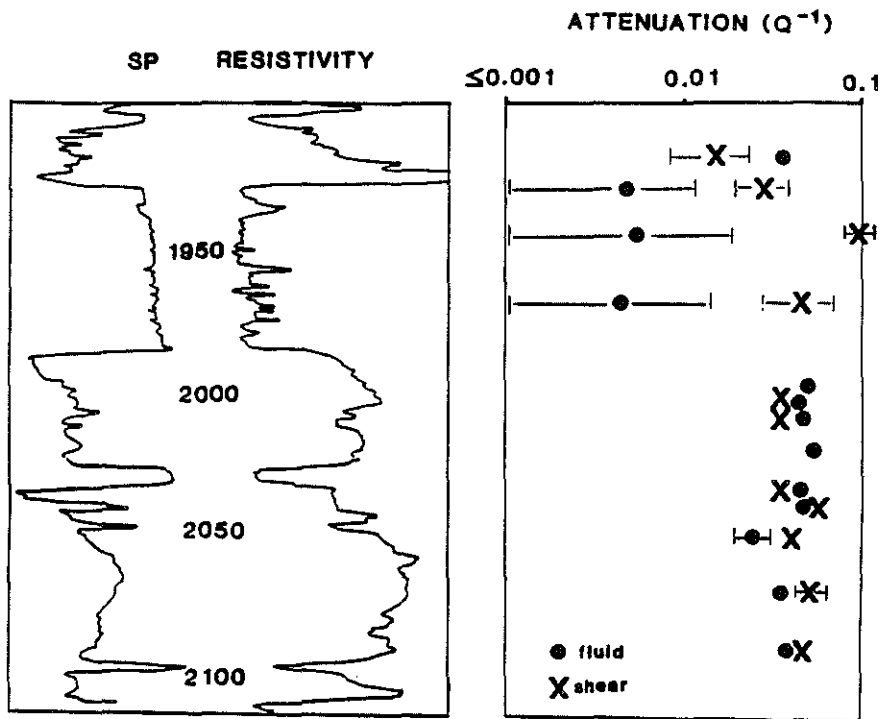
Burns and Cheng

Figure 13: Plot of the estimated attenuation values for the sand/shale example. The fluid attenuation values are given by the solid dots, and the formation shear wave attenuation values are given by the x's. Representative error bars (+- one standard deviation) are also indicated

Table 4: Inversion results for the sand/shale data example

DEPTH	$Q_f^{-1}(x10^{-2})$	$Q_\beta^{-1}(x10^{-2})$
1920	3.64 +- 0.550	1.59 +- 0.756
1930	0.468 +- 0.69	2.87 +- 0.927
1946	0.557 +- 1.38	9.83 +- 1.99
1970	0.449 +- 1.01	4.97 +- 2.10
2000	4.72 +- 0.513	4.49 +- 1.33
2003	4.57 +- 0.483	3.51 +- 0.934
2010	4.68 +- 0.431	3.61 +- 0.817
2020	5.20 +- 0.442	4.37 +- 1.01
2035	4.10 +- 0.477	3.57 +- 0.755
2040	4.69 +- 0.717	5.20 +- 1.40
2050	2.51 +- 0.592	4.07 +- 1.01
2070	4.53 +- 0.601	2.31 +- 0.364
2090	4.01 +- 0.426	4.26 +- 0.720

to both physical and numerical inadequacies in the model. The sand intervals in this well have shear wave velocities which are greater than the fluid velocity, that is they are fast formations. The shale intervals have lower shear velocity values, and in most cases can be classified as 'slow' formations. The model behavior (partition coefficients) is very dependent on the ratio of the shear wave velocity to the fluid velocity (Burns, 1986). In a 'slow' formation, the Stoneley wave attenuation is sensitive to both the fluid and formation shear Q values in approximately equal measure, with the formation shear Q becoming more dominant with increasing frequency. In a fast formation, however, the Stoneley wave attenuation is much more sensitive to the fluid Q value and the partition coefficients are almost invariant with frequency. In such situations, the Stoneley wave amplitude information can provide good estimates of the fluid Q value, but the pseudo-Rayleigh wave is needed to estimate the formation shear wave Q with any confidence. The small diameter of the borehole in this example, together with the low frequency source, resulted in no pseudo-Rayleigh wave excitation. It is not too surprising, then, that the Stoneley wave attenuation in the fast formation sand units is not adequate to estimate both the fluid and formation shear wave Q values. Data resolution calculations indicate that the model can only match the average Stoneley attenuation value of the data in the frequency range used. The partition coefficient values in these zones are about 0.7 for the fluid compressional energy and about 0.25 for the formation shear energy, with variations of only a few percent over the frequency band used. The inversion routine, in these zones, is basically trying to fit two unknowns $(Q_f^{-1}$ and $Q_\beta^{-1})$ to a single data point, with the result being very poor parameter resolution.

The Stoneley wave attenuation does a much better job in the slow formation shales. In these intervals, the fluid and formation shear wave partition coefficients are of the same order (0.4 - 0.55) and show greater variation with frequency. The resulting parameter estimates are better resolved and more reliable.

The damping factor can be adjusted in the sand intervals to force the fluid Q values to agree with those obtained in the shale zones. The resulting formation shear wave Q values, however, become unrealistically low ($Q_\beta = 4$-10). This leads to the second reason for the inconsistencies between the sand and shale zone inversion results: losses due to fluid flow in the permeable sand units. The sandstone intervals (depth interval 1990 - 2100) in this well have extremely high permeability values (100 - 3000 millidarcies(md)). Several authors (Williams et al., 1984; Zemanek et al., 1985) have shown that very good correlations exist between Stoneley (tube) wave attenuation (amplitude ratio) and permeability in field recorded data. Correlations exist between the tube wave velocity and permeability as well. Several other authors (Schmitt, 1985; Hsui et al., 1986; Cheng et al., 1987; Burns and Cheng, 1986) have used the Biot theory of wave propagation in porous and permeable formations to try to explain these correlations with some success. The very high permeability associated with the sandstone intervals of this well results in additional attenuation of the Stoneley wave due to energy coupling between the borehole fluid and the pore fluid of the permeable formation. The model used in the inversion procedure, however, does not explicitly address this attenuation mechanism. The increased attenuation in these zones, therefore, is reflected in the much lower fluid Q value estimates.

Limestone/Dolomite Example

The second real data application involves full waveform acoustic logs recorded in a deep borehole that penetrated a limestone-dolomite lithologic section. The borehole diameter is 0.219 m (8.625"), and the drilling fluid in this example was reported to consist of a dispersed gel (in water) with a density of 1.2 gm/cc and an estimated velocity of 1525 m/sec (5000 ft/sec). The lithology varies between low porosity limestone (0-3%) and higher porosity dolomite (5-15%) in the interval from 1570 m (5150') to 1616 m (5300')(note: the depths are relative to an arbitrary reference and not the actual values). Again, data from a number of depths have been selected through this interval. The depths and model input parameters are given in Table 5. Formation P and S wave velocities were obtained from the full waveform acoustic logs. The data from this borehole was collected with the same downhole tool as the previous example (source-receiver offsets of 4.57m (15') and 6.1m (20')). The data traces for two of the depths used are shown in Figure 14. Because this example consists of a fast formation, and the borehole radius is sufficiently large to result in the excitation of the pseudo-Rayeigh wave in the source frequency band, both the Stoneley and pseudo-Rayleigh wave spectral

Table 5: Depth and model parameters used for the limestone/dolomite data example

DEPTH	V_p (m/sec)	V_s (m/sec)	ρ (g/cm^3)
5165	6353	3388	2.71
5180	5543	3388	2.65
5210	5349	3388	2.57
5213	5543	3278	2.57
5225	5256	3143	2.50
5230	5276	3278	2.55
5239	5863	3243	2.62
5250	6353	3388	2.72
5265	6098	3783	2.62
5275	6353	3465	2.70
5290	5752	3388	2.70

ratios are used in the inversion.

The results of the inversion for this data set are given in Table 6. A five point centered running average has been used to smooth the amplitude spectra in this example. As in the previous example, a small amount of damping has been used in some cases. The fluid Q estimates are very consistent (fluid Q = 25 - 40) and very well resolved (fluid Q resolution = 0.9 - 1.0). This is due to the Stoneley wave attenuation which is completely dominated by the fluid attenuation value for this very rigid, fast formation (fluid partition coefficients = 0.93 - 0.95). The data resolution is similar to what was seen for the cased hole synthetic example. The Stoneley wave Q^{-1} data is basically invariant with frequency and is completely dominated by the fluid attenuation. The pseudo-Rayleigh wave attenuation is sensitive to the formation shear wave attenuation at frequencies very close to the cutoff frequency (about 9kHz), but the sensitivity decreases rapidly with increasing frequency. This rapid drop off of sensitivity results in the formation shear Q estimates being very sensitive to the spectral ratio data in a narrow frequency band near the cutoff frequency. Figure 15 shows the amplitude spectra for one representative depth with and without the running average imposed. The Stoneley wave data is very stable, but the pseudo-Rayleigh wave data is very noisy, especially in the vicinity of the cutoff frequency. The low frequency source (centered around 3-6kHz) has low energy in the pseudo-Rayleigh frequency band, making the amplitude information in this band sensitive to the background noise level. This fact, coupled with the lower excitation amplitude of the pseudo-Rayleigh wave near the cutoff frequency (Burns, 1986), results in spectral ratios which are noisy in this critical frequency band. The result of this noise sensitivity is generally poor resolution of the formation shear
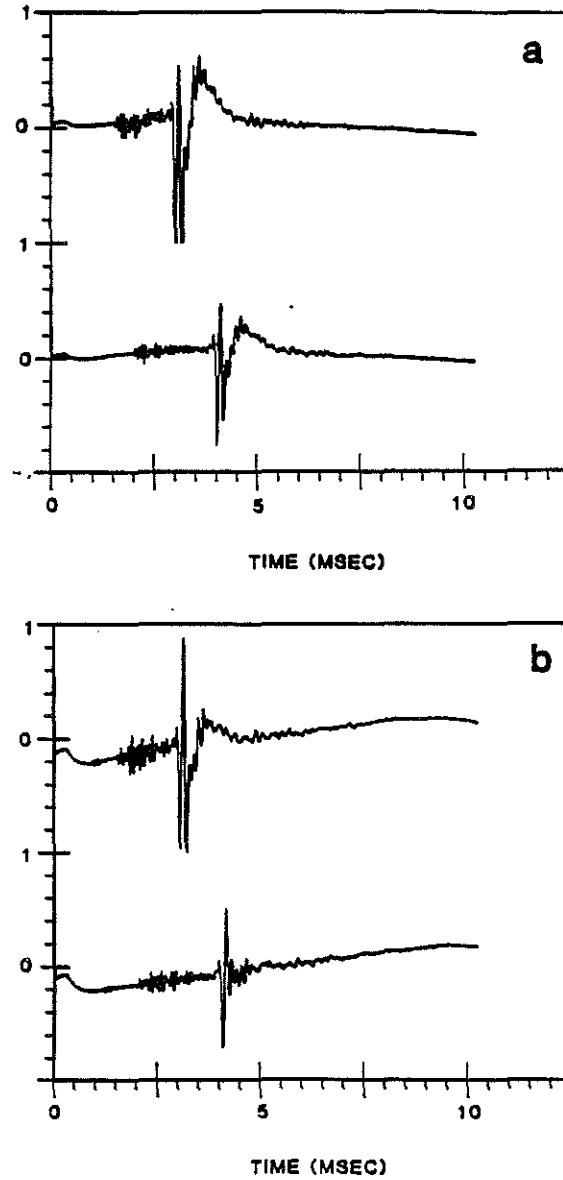
Burns and Cheng

Figure 14: Near (4.57m, 15') and far (6.1m, 20') offset traces for two depths of the limestone example full waveform acoustic log data: (a) depth 5165 and (b) depth 5290. Both traces in each example are normalized to the maximum amplitude of the near offset trace

Table 6: Inversion results for the limestone/dolomite data example

DEPTH	$Q_f^{-1}(x10^{-2})$	$Q_\beta^{-1}(x10^{-2})$
5165	2.015 +- 0.255	2.54 +- 1.47
5180	2.80 +- 0.382	1.25 +- 1.26
5210	4.55 +- 0.322	1.97 +- 0.86
5213	2.21 +- 0.264	0.497 +- 0.805
5225	2.44 +- 0.482	3.28 +- 2.05
5230	2.79 +- 0.374	1.67 +- 1.07
5239	2.75 +- 0.394	3.20 +- 1.39
5250	1.83 +- 0.290	1.49 +- 1.10
5265	1.30 +- 0.117	4.89 +- 0.489
5275	1.03 +- 0.158	2.28 +- 0.35
5290	3.85 +- 0.266	1.11 +- 0.658

wave Q values. The spectral smoothing, however, helps reduce the noise problems and improves the resolution of the solutions.

The estimated Q values for this example are fairly consistent. The fluid Q estimates are well resolved and consistent in both the limestone and dolomite sections. The values are lower than the values found in the last example (fluid Q = 25 - 40), reflecting the differences in the borehole fluid for the two examples. The formation shear wave Q estimates also show consistency within the data set. The Q_β values in this example are much higher than in the previous example (shear Q = 60 - 120). Little variation in Q_β values between the limestone and dolomite intervals is evident. Figure 16 gives the estimated Q values with error bars over the interval of interest. Borehole measurements of formation density and natural gamma radiation are also given in this figure.

The porous dolomite intervals in this example are also permeable. The permeability values in this well, however, are much lower than in the previous example (0 - 20 md). The Q estimates in the porous interval (5200 - 5250) do not show a dramatic decrease over the values in the non-porous limestone, although the fluid Q estimates do show a slight decrease which may be attributed to the fluid flow losses in these zones.

CONCLUSIONS

The energy partition coefficient model, developed by Cheng et al. (1982) and adapted to multilayered borehole geometries by Burns et al. (1985), was applied to the problem
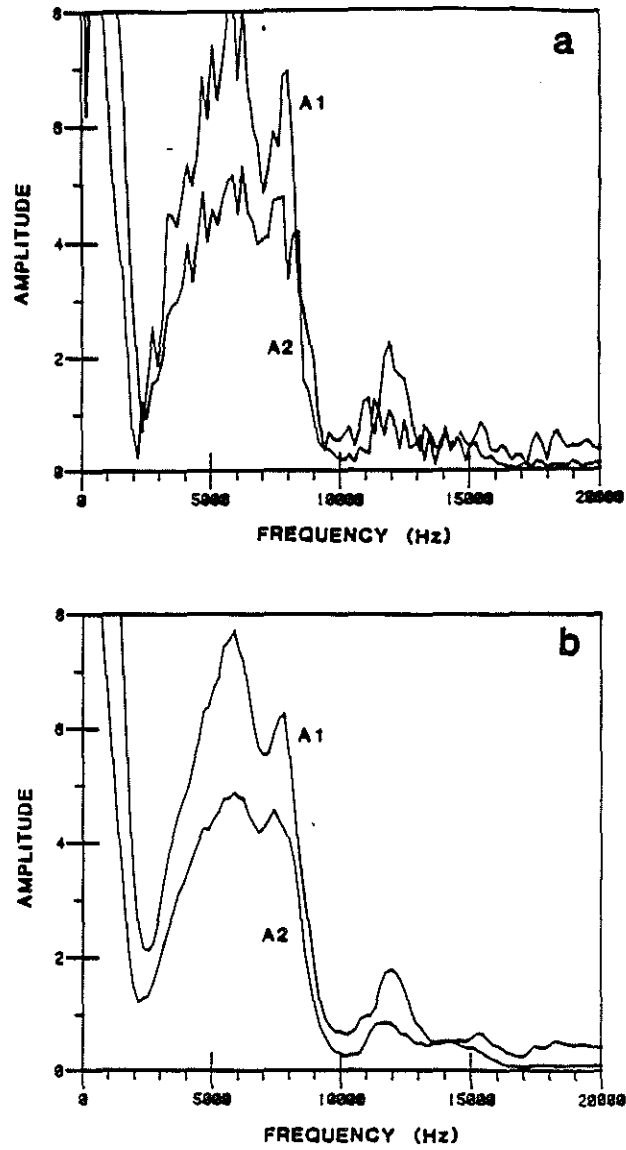
Burns and Cheng

Figure 15: Amplitude spectra (a)without and (b) with a five point (centered) running average applied. Spectra correspond to the depth of 5165 in the limestone example
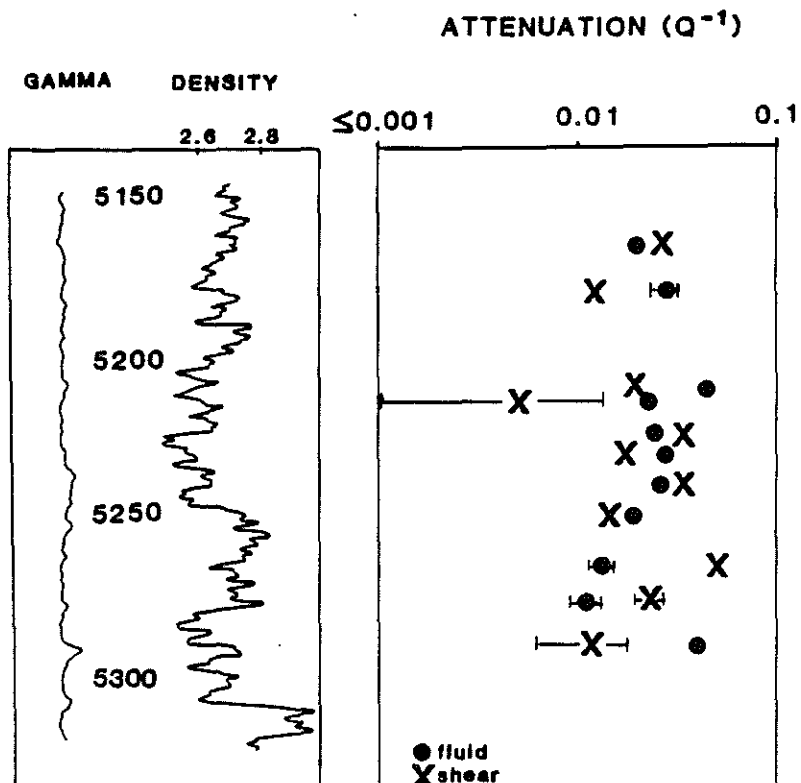
Figure 16: Plot of the estimated attenuation values for the limestone/dolomite example. The fluid attenuation values are given by the solid dots, and the formation shear wave attenuation values are given by the x's. Representative error bars (+- one standard deviation) are also indicated

of estimating formation Q_β from borehole guided waves. A linear damped least squares inversion routine was developed to simultaneously invert Stoneley and pseudo-Rayleigh wave spectral ratio data for Q_f^{-1} and Q_β^{-1} in open hole geometries, and Q_f^{-1}, Q_β^{-1}, and $Q_{\beta_{cmt}}^{-1}$ in cased hole geometries. Inversion of synthetic waveform data indicated that in open hole situations the procedure provides excellent results although the fluid velocity, formation shear wave velocity, and the borehole radius parameters must be known with an accuracy of a few percent. Synthetic cased hole data inversion resulted in excellent estimates of the fluid Q and cement shear wave Q values, but the accuracy of the formation shear wave Q estimate is especially dependent on the spectral ratio measurements very close to the cutoff frequency.

The inversion method was also applied to field data examples in two different lithologic sections. In the first example, fluid Q and formation shear wave Q estimates were obtained in a sand-shale sequence using the Stoneley wave only. The formation S wave velocities in this data set were fairly low, varying between values just below the fluid velocity to values just above the fluid velocity. The Stoneley wave attenuation in this data was quite sensitive to the formation shear wave Q in the 'slow' formation regions, but less sensitive in the faster sandstone units. The Q estimates in the 'slow' shale units were quite reasonable, while the estimates in the highly permeable sandstone intervals were substantially lower due to fluid flow losses. The second field data example was in limestone-dolomite sequence. The formation velocities in this example were very high, and the Stoneley and pseudo-Rayleigh wave spectral ratios were used simultaneously in the inversion. The results of this example were similar to the cased borehole synthetic result: the Q_β estimates are sensitive to the quality of the pseudo-Rayleigh spectral ratio data very close to the cutoff frequency. The pseudo-Rayleigh wave in this frequency region has low excitation amplitude, and is very sensitive to noise contamination. Spectral smoothing helped to alleviate some of the noise problems. The fluid Q estimates obtained in this example were well resolved and consistent, as were the formation shear wave Q estimates.

ACKNOWLEDGEMENTS

REFERENCES

Aki, K. and Richards, P., 1980, Quantitative Seismology: Theory and Methods, v.I and v.II; W. H. Freeman and Co., San Francisco.

Burns, D.R., 1986, Formation property estimation from guided waves in a borehole; Ph.D. Thesis, Massachusetts Institute of Technology, Cambridge, MA.

Burns, D.R. and Cheng, C.H., 1986, Determination of in-situ permeability from tube wave velocity and attenuation; Trans. SPWLA 27th Ann. Logging Symp., paper KK.

Burns, D.R., Cheng, C.H., and Toksöz, M.N., 1985, Energy partitioning and attenuation of guided waves in radially layered boreholes; expanded abstracts of the 55th Annual SEG Meeting, Washington, D.C.

Cheng, C.H. and Toksöz, M.N., 1981, Elastic wave propagation in a fluid-filled borehole and synthetic acoustic logs; Geophysics, 46, 1042–1053.

Cheng, C.H., Toksöz, M.N. and Willis, M.E., 1982, Determination of in-situ attenuation from full waveform acoustic logs; J. Geophys. Res., 87, 5477–5484.

Cheng, C.H., Wilkens, R.H., and Meredith, J.A., 1986, Modelling of full waveform acoustic logs in soft marine sediments; Trans. SPWLA 27th Ann. Logging Symp., paper LL.

Cheng, C.H., Zhang, J., and Burns, D.R., 1987, Effects of in-situ permeability on the propagation of Stoneley (tube) waves in a borehole; Geophysics, in press.

Hsui, A.T., Zhang, J., Cheng, C.H., and Toksöz, M.N., 1985, Tube wave attenuation and in-situ permeability; Trans. SPWLA 26th Ann. Logging Symp., paper CC.

Johnston, D.H., 1978, The attenuation of seismic waves in dry and saturated rocks; Ph.D. Thesis, Massachusetts Institute of Technology, Cambridge, MA.

Johnston, D.H., Toksöz, M.N., and Timur, A., 1979, The attenuation of seismic waves in dry and saturated rocks: II. mechanisms; Geophysics, 44, 691–711.

Lines, L.R. and Treitel, S., 1984, Tutorial: a review of least squares inversion and application to geophysical problems; Geophys. Prosp., 32, 159–186.

Rosenbaum, J.H., 1974, Synthetic microseismograms: logging in porous formations; Geo-

physics, 39, 14–32.

Schmitt, D.P., 1985, Simulation numerique de diagraphies acoustiques propagation d'ondes dans des formations cylindriques axisymetriques radialement stratifees incluant des millieux elastiques et/ou poreux satures; Ph.D. Thesis, University of Grenoble, Grenoble, France.

Toksöz, M.N., Johnston, D.H., and Timur, A., 1979, Attenuation of seismic waves in dry and saturated rocks: I. laboratory measurements; Geophysics, 44, 681–690.

Tsang, L. and Rader, D., 1979, Numerical evaluation of transient acoustic waveform due to a point source in a fluid-filled borehole; Geophysics, 44, 1706–1720.

Tubman, K.M., 1984, Synthetic full waveform acoustic logs in radially layered boreholes; Ph.D. Thesis, Massachusetts Institute of Technology, Cambridge, MA.

White, J.E. and Zechman, R.E., 1968, Computed response of an acoustic logging tool; Geophysics, 33, 302–310.

Wiggins, R.A., 1972, General linear inverse problem — implication of surface waves and free oscillations for earth structure; Rev. of Geophy. and Space Phys., 10, 251–285.

Williams, D.M., Zemanek, J., Angona, F.A., Dennis, C.L., and Caldwell, R.L., 1984, The long space acoustic logging tool; Trans. SPWLA 25th Ann. Logging Symp., Paper T.

Willis, M.E., 1983, Seismic velocity and attenuation from full waveform acoustic logs; Ph.D. Thesis, Massachusetts Institute of Technology, Cambridge, MA.

Willis, M.E., and Toksöz, M.N., 1983, Automatic P and S velocity determination from full waveform acoustic logs; Geophysics, 48, 1631–1644.

Winkler, K. and Nur, A., 1979, Pore fluids and seismic attenuation in rocks; Geophy. Res. L., 6, 1–4.

Zemanek, J., Angona, F.A., Williams, D.M., and Caldwell, R.L., 1984, Continuous acoustic shear wave logging; Trans. SPWLA 25th Ann. Logging Symp., paper U.

Zemanek, J., Williams, D.M., Caldwell, R.L., Dennis, C.L., and Angona, F.A., 1985, New developments in acoustic logging; presented at the Indonesian Pet. Assoc. 14th Ann. Conv.